Radiative Properties of Boundary Layer Clouds: Droplet Effective Radius versus Number Concentration

JEAN-LOUIS BRENGUIER AND HANNA PAWLOWSKA*

Météo-France, CNRM-GAME, GMEI, Toulouse, France

LOTHAR SCHÜLLER, RENE PREUSKER, AND JÜRGEN FISCHER

Institut für Weltraumwissenschaften, Freie Universität Berlin, Berlin, Germany

YVES FOUQUART

Laboratoire d'Optique Atmosphérique, Université des Sciences et Techniques de Lille, Lille, France

(Manuscript received 24 June 1998, in final form 4 May 1999)

ABSTRACT

The plane-parallel model for the parameterization of clouds in global climate models is examined in order to estimate the effects of the vertical profile of the microphysical parameters on radiative transfer calculations for extended boundary layer clouds. The vertically uniform model is thus compared to the adiabatic stratified one. The validation of the adiabatic model is based on simultaneous measurements of cloud microphysical parameters in situ and cloud radiative properties from above the cloud layer with a multispectral radiometer. In particular, the observations demonstrate that the dependency of cloud optical thickness on cloud geometrical thickness is larger than predicted with the vertically uniform model and that it is in agreement with the prediction of the adiabatic one. Numerical simulations of the radiative transfer have been performed to establish the equivalence between the two models in terms of the effective radius. They show that the equivalent effective radius of a vertically uniform model is between 80% and 100% of the effective radius at the top of an adiabatic stratified model. The relationship depends, in fact, upon the cloud geometrical thickness and droplet concentration. Remote sensing measurements of cloud radiances in the visible and near infrared are then examined at the scale of a cloud system for a marine case and the most polluted case sampled during the second Aerosol Characterization Experiment. The distributions of the measured values are significantly different between the two cases. This constitutes observational evidence of the aerosol indirect effect at the scale of a cloud system. Finally, the adiabatic stratified model is used to develop a procedure for the retrieval of cloud geometrical thickness and cloud droplet number concentration from the measurements of cloud radiances. It is applied to the marine and to the polluted cases. The retrieved values of droplet concentration are significantly underestimated with respect to the values measured in situ. Despite this discrepancy the procedure is efficient at distinguishing the difference between the two cases.

1. Introduction

The earth radiation budget is strongly modulated by clouds that reflect solar radiation and absorb longwave thermal emission from the earth. The net effect is a cooling of the climate system, with the main contribution coming from marine boundary layer (BL) clouds. Their high albedos (30%–40%) compared with the ocean background (10%) give rise to large deficits in the absorbed solar radiative flux at the top of the atmosphere, while their low altitude prevents significant compensation in thermal emission (Randall et al. 1984). The prospect of a global warming (2°–3°C) due to the doubling of CO_2 during the industrial era has been tempered by the identification of a radiative forcing mechanism involving clouds. For the same spatial distribution of liquid water content (LWC), a cloud made of numerous small droplets reflects more (higher albedo) than a cloud with fewer but larger droplets. The droplet number concentration (N) in a cloud (and therefore the mean droplet size at constant LWC) is dependent upon the number concentration of the cloud condensation nuclei (CCN) at the cloud base. The release of greenhouse

* Additional affiliation: Institute of Geophysics, University of Warsaw, Warsaw, Poland.

Corresponding author address: Dr. J. L. Brenguier, Météo-France, Centre National de Recherches Meteorologiques, GMEI/MNP, 42 av. Coriolis, 31057 Toulouse Cedex 01, France.
E-mail: jlb@meteo.fr

gases has been concomitant with an increase of anthropogenic aerosols, either released directly into the atmosphere or generated in situ by the transformation and condensation of primary pollutants, such as SO_2. These particles can act as CCN (Twomey 1977), increasing N and therefore the cloud albedo. This forcing, referred to as the indirect effect of aerosols, is likely to counteract part of the warming due to greenhouse gases (Slingo 1990; Jones et al. 1994).

The overall indirect effect of the aerosols on climate change is far from being precisely evaluated, though the sign is thought to be negative (stable coupling). The difficulty in assessing the importance of the indirect effect on climate change arises from the small time and spatial scales involved in the CCN, cloud microphysics, cloud dynamics, and radiation interactions, while global climate models (GCMs) simulate the average and long-term effects of clouds. In addition to the forcing by aerosols, possible feedback mechanisms involving clouds have also been identified. These include the extension of cloud cover prompted by a rise of the global temperature (Arking 1991), the enhancement of natural CCN production by planktonic algae at higher ocean surface temperature (Charlson et al. 1987; Boers et al. 1998), reduction of cloud precipitation efficiency due to smaller droplets and resulting in a longer cloud life time (Albrecht, 1989), the effect of precipitation on CCN distributions (Ackerman et al. 1993), the coupling between diabatic processes and cloud dynamics (Pincus and Baker 1994; Martin et al. 1997), and the radiative effect of in-cloud absorption on shortwave radiation (Boers and Mitchell 1994).

In order to simulate such a complex system of mutual interactions in GCMs, it is crucial to develop parameterizations based on processes rather than empirical formulas. The essence of the processes must be captured in the parameterizations, and empirical tuning must be limited to coefficients that are not likely to be affected by the coupling. However, it is also useless to base a parameterization on variables that cannot be diagnosed by a GCM.

For the simulation of the aerosol indirect effect and cloud feedback, there are four types of processes to take into account. (i) *Cloud generation* includes the diagnostic of the integrated liquid water content in the GCM grid, its statistical distribution within the grid (cloud fraction), the geometrical cloud thickness, and cloud-base and -top altitudes. These parameters can be diagnosed by a GCM with subgrid parameterization of cloud cover (Del Genio et al. 1996). (ii) *Aerosol properties* include the prognostic of aerosol contents and physical properties such as their activation spectrum. They can be obtained with aerosol transport models, which for the moment are run offline the GCM (Langner and Rodhe 1991). (iii) *Aerosol–droplets interaction* refers to the CCN activation process that is strongly dependent upon the nucleation properties of CCN and the updraft intensity at cloud base. A characteristic updraft velocity can be estimated via the turbulent kinetic energy in a grid and a parameterization of its statistical distribution at the cloud base. With aerosol nucleation properties derived in (ii), such a parameterization provides a typical value of N in clouds. (iv) *Cloud radiative parameterizations* relate the morphological properties of clouds and their internal microphysics to the mean radiative properties at the grid scale. The feedback mechanism involving precipitation efficiency establishes a link between the droplet concentration derived in (iii) and cloud generation schemes (i). The droplet concentration influences the conversion rate of condensation droplets into precipitating particles and, therefore, the rate of removal of LWC from the cloud layer in a GCM model.

Radiative transfer calculations via the doubling–adding matrix method (Twomey et al. 1966) or the two-stream approximation (Coalkley and Chýlek 1975; Stephens 1978; Slingo and Schrecker 1982) are controlled by two cloud parameters, the liquid water path (LWP), and the droplet effective radius (r_e). LWP is the integral of LWC over the cloud depth and it is diagnosed by the model. In the early schemes the value of the effective radius is fixed (Letreut and Li 1991) or depends on the cloud depth (Fouquart et al. 1990; McFarlane et al. 1992) so that there is no consideration about possible effects due to the aerosols. The next step has been to select different values of r_e depending on the geographical location of the clouds: $13 \approx 14$ μm over the ocean and $9 \approx 10$ μm over the continent (Bower and Choularton 1992).

With the calculation of the transport and transformation of the aerosols in GCMs and the prediction of their nucleating properties, it starts to be appropriate to develop parameterizations based on droplet concentration, a parameter which can be directly linked to the aerosol properties. Locally LWC and the droplet sizes are related to the droplet number concentration N via

$$w = (4/3)\pi\rho_w N r_v^3, \tag{1}$$

where w is the liquid water content, ρ_w is the liquid water density, and r_v is the mean volume radius of the droplet spectrum. Various formulas have been proposed in the literature for deriving the optical thickness τ from LWP and the droplet concentration, with a correction factor for the difference between the mean volume and the effective radii (Fouquart et al. 1990; Bower and Choularton 1992; Raga and Jonas 1993b; Jones et al. 1994; Han et al. 1994). These formulas have been tested with in situ observations of the cloud microphysics (Raga and Jonas 1993a; Gultepe et al. 1996). However, the cloud optical thickness is the vertical integral of the ratio w/r_e, which depends upon the vertical profiles of these two quantities. The parameterizations mentioned above have been developed by assuming a constant effective radius through the cloud depth, while observations clearly show that the effective radius is increasing with the altitude above cloud base (Slingo et al. 1982;

Nicholls 1984; Stephens and Platt 1987; Raga and Jonas 1993a; Martin et al. 1994).

Radiative transfer calculations are often performed by assuming that a cloud is a horizontally and vertically uniform plane-parallel layer. Such models will be hereafter referred to as the vertically uniform plane-parallel model (VU-PPM) in the paper. The effects of horizontal inhomogeneity have been largely tested with statistical models of microphysical variability and especially fractal models (Barker 1992; Cahalan et al. 1994a; Cahalan et al. 1994b; Cahalan et al. 1995; Davis et al. 1996; Duda et al. 1996; Barker 1996). It has been demonstrated that the albedo of inhomogeneous clouds is smaller than the albedo of a homogeneous plane-parallel cloud with the same horizontally averaged LWP. The effects of vertical stratification of the microphysics have not been so carefully evaluated (Li et al. 1994). In fact, aircraft measurements are limited for such characterizations because the variability of the microphysics in the horizontal dimension complicates their interpretation. Large samples are thus needed in order to extract information on the microphysics–radiation interaction. For example, the results reported by Boers et al. (1998) are based on the analysis of 12 flights (six during the winter season and six during the summer season). The respective contributions of the LWP and the effective radius are clearly distinguished, and the change in albedo due to the change in droplet concentration between summer and winter clouds can be estimated. This provides the first experimental evidence of the Twomey effect at the scale of a cloud system.

The purpose of this paper is to demonstrate that the vertical stratification of the cloud microphysics should be taken into account in GCM parameterizations and that it can be well approximated with the adiabatic cloud model for radiative transfer calculations. We therefore begin (section 2) with a presentation of the basic formalism for microphysics–radiation interaction. The main difference with previous experimental studies is in the size of the dataset for characterizing actual profiles. The analysis of the two cases presented here, 26 June 1997, for the marine reference, and 9 July 1997, as an example of a polluted case, are based on, respectively, 35 and 28 profiles flown through the cloud layer with an instrumented aircraft. The observations have been performed during the CLOUDYCOLUMN Project of the Second Aerosol Characterization Experiment (ACE-2), in June and July 1997, north of the Canary Islands. The objectives of the project and the experimental strategy are briefly presented in section 3. We also summarize observations of the vertical stratification of the microphysics and analyze microphysical properties in subadiabatic cloud regions. The main difference between a VU-PPM and an adiabatic stratified cloud model is in the dependence of the optical thickness on the cloud geometrical thickness. This feature is tested in section 4 to validate the adiabatic stratified model. This model will be hereafter referred to as the adiabatic stratified plane-parallel model (AS-PPM). The VU-PPM is, however, an attractive model because of its simplicity. Radiative transfer calculations are thus discussed in section 5 in order to identify a possible equivalence between the VU- and the AS-PPMs. The AS-PPM is not only more realistic than the VU-PPM for the description of the cloud microphysics; it also provides a way of deriving, from remote sensing of the multispectral radiances, an estimation of the droplet concentration instead of the effective radius as with a VU-PPM. The procedure is illustrated in section 6. The discussion in section 7 summarizes the potential applications of the AS-PPM, and the conclusions are presented in section 8.

2. GCM parameterizations of cloud radiative properties

a. Radiative properties of a homogeneous cloud volume

The radiative properties of a homogeneous cloud volume in the shortwave range (SW) are parameterized with only three parameters: the extinction coefficient $\sigma_{\text{ext}} = \sigma_{\text{abs}} + \sigma_{\text{sc}}$, where σ_{abs} refers to absorption and σ_{sc} to scattering; the single-scattering albedo $\omega = \sigma_{\text{sc}}/\sigma_{\text{ext}}$; and the scattering phase function $p(\theta)$, which is the probability of scattering in a direction θ with respect to the incident direction. In GCM radiation codes, one often uses the asymmetry factor $g = \int_0^{2\pi} p(\theta) \cos\theta \, d\theta$ ($g = 1$ for forward scattering and $g = 0$ for isotropic scattering), though the complete phase function is required for accurate calculations such as presented in sections 5 and 6.

The extinction is proportional to the total droplet surface per unit volume of air (Hansen and Travis 1974; Stephens 1978):

$$\sigma_{\text{ext}} = \int_0^{\infty} Q_{\text{ext}}(x)\pi r^2 n(r)\, dr = \pi Q_{\text{ext}}(\overline{x}) N r_s^2, \quad (2)$$

where $x = 2\pi r/\lambda$ is the size parameter, $\overline{x}$ is its effective mean value, Q_{ext} is the Mie efficiency factor (van de Hulst 1957), $N = \int_0^{\infty} n(r)\, dr$ is the droplet number concentration, and r_s is the mean surface radius of the droplet size distribution. For large values of x, Q_{ext} becomes asymptotic approaching a value of approximately 2. This value will be further used in this paper for data analysis.

It has also been demonstrated that the three radiative parameters can be approximated as functions of the LWC and the effective radius of the droplet size distribution, $r_e = r_v^3/r_s^2$ (Hansen and Travis 1974; Twomey and Cocks 1989). For example, Slingo and Schrecker (1982) have derived a parameterization for 24 spectral bands covering the SW from $\lambda = 0.25$ to 4 μm:

$$\sigma_{\text{ext},i} = w\left(a_i + \frac{b_i}{r_e}\right), \tag{3}$$

$$\omega_i = 1 - c_i - d_i r_e, \tag{4}$$

$$g_i = e_i + f_i r_e, \tag{5}$$

where the coefficients a_i to f_i are dependent upon the spectral band. At this point, the parameterization provides simple relationships between the microphysical characteristics (w and r_e), and the radiative properties of a homogeneous cloud volume (σ_{ext}, ω, and g).

b. Radiative properties of a homogeneous cloud: Plane-parallel model

Tests of the parameterization described above and detailed calculations of the heating rate profiles have been performed with realistic vertical profiles of w and r_e in horizontally homogeneous clouds (Slingo and Schrecker 1982). However, it is not feasible to enter so many details into a GCM parameterization. Therefore, the radiative transfer is often parameterized by assuming that the cloud is also vertically uniform with a geometrical thickness H (VU-PPM). For example, Slingo (1989) extended the above parameterization [Eqs. (3)–(5)] for a homogeneous cloud volume to a VU-PPM. In this case the parameterization becomes

$$\langle \tau_i \rangle = W\left(a_i + \frac{b_i}{\langle r_e \rangle}\right) \tag{6}$$

$$\langle \omega_i \rangle = 1 - c_i - d_i \langle r_e \rangle \tag{7}$$

$$\langle g_i \rangle = e_i + f_i \langle r_e \rangle, \tag{8}$$

where $\tau = \int_0^H \sigma_{\text{ext}}(h)\, dh$ is the cloud optical thickness, $W = \int_0^H w(h)\, dh$ is the liquid water path, h is the altitude above cloud base, and $\langle\ \rangle$ refers to the VU-PPM equivalent parameters.

There is currently a general consensus on parameterizations of cloud radiative properties based on LWP and effective radius. Cloud geometrical thickness and droplet number concentration are not explicitly used as variables. They rather appear implicitly in the derivation of the above parameters. The relation between r_v and r_e, which depends upon the droplet spectral shape, has been derived from in situ measurements that suggest that the ratio $k = r_v^3/r_e^3$ varies from 0.67 ± 0.07 in continental air masses to 0.80 ± 0.07 in marine ones (Pontikis and Hicks 1992; Martin et al. 1994).

VU-PPM based parameterizations cover a wide range of applications, such as numerical studies of the climate feedback and indirect effect with GCMs (Fouquart and Bonnel 1980; Slingo 1989; Jones et al. 1994), and validation tests of techniques for the retrieval of cloud parameters from satellite measurements of cloud reflectance (Twomey and Cocks 1989; Nakajima and King 1990; Platnick and Twomey 1994; Han et al. 1994; Platnick and Valero 1995). However, the VU-PPM hypothesis raises the question of the definition of the VU-PPM parameters equivalent to a realistic cloud. Formally, the solution is not straightforward because σ_{ext} is a linear function of $1/r_e$ while ω and g are linear functions of r_e. In addition, the effects of σ, ω, and g on radiative transfer calculations are not linear (Li et al. 1994). The recent literature on this subject reveals no consensus: in Taylor and McHaffie (1994), ''the cloud top r_e should be used since the albedo is dependent on the cloud-top value'' [$\langle r_e \rangle = r_e(H)$]; in Nakajima et al. (1991) and in Platnick and Twomey (1994), ''droplet sizes near cloud top contribute a greater influence to the inferred sizes than droplets farther down in the cloud'' [the upper 20%–40% of the cloud layer, in Nakajima and King (1990)]; in Stephens and Platt (1987) and in Li et al. (1994), ''this should be done by comparing measured reflectance spectra to those computed using mean microphysical parameters'' [$\langle r_e \rangle = \overline{r_e(h)}$, where the overbar indicates a vertical average over H]; in Han et al. (1994), ''the results are sensitive to droplet sizes in the uppermost one or two units of cloud optical thickness'' [the upper two to three units of cloud optical thickness in Platnick and Valero (1995)].

From microphysical measurements in stratocumulus reported in the literature (see next section), the relative difference between these various solutions for the VU-PPM equivalent effective radius can reach up to 30%. This is quite large when compared to the accuracy of 10^{-3} in the calculation of the coefficients a_i to f_i in Eqs. (3)–(5) (Slingo 1989). This is also large when compared to the accuracy that is needed for validation of satellite effective radius retrieval techniques. For example, Platnick and Valero (1995) estimate that the worst case net uncertainty in their retrieval technique ranges from −20% to +25% (or absolute uncertainty from about −2.3 to +3.0 μm).

c. Radiative properties of an adiabatic cloud column

The adiabatic model describes the microphysical evolution of a convective closed parcel of moist air. At cloud base, the water vapor mixing ratio reaches saturation. During the convective ascent, the temperature of the air decreases according to the pseudoadiabatic lapse rate. The saturation water vapor mixing ratio decreases accordingly. The adiabatic liquid water content at the altitude h above cloud base $w_{\text{ad}}(h)$ is defined as the difference between the saturation water vapor mixing ratio at the cloud base and its value at the level h. The value of $w_{\text{ad}}(h)$ is increasing almost linearly with altitude, since the moist adiabatic condensate coefficient C_w is constant over a short altitude range such as through stratocumulus clouds with a depth smaller than 1 km (Brenguier 1991). Its value, which depends slightly on the temperature in the cloud layer, ranges from 1 to 2.5 × 10^{-3} g m^{-4} for a temperature between 0° and 40°C (ibid, Fig. 3). In addition, the adiabatic droplet concen-

tration N_{ad} is constant in a nonprecipitating adiabatic parcel; hence,

$$w_{ad}(h) = C_w h, \tag{9}$$

$$r_{vad}(h) = (Ah)^{1/3} N_{ad}^{-1/3}, \quad \text{with } A = \frac{C_w}{(4/3)\pi\rho_w}, \tag{10}$$

$$r_{ead}(h) = k^{-1/3} r_{vad} = (Ah)^{1/3}(kN_{ad})^{-1/3} \quad \text{and}$$

$$r_{sad} = k^{1/6} r_{vad}, \tag{11}$$

where the subscript ''ad'' in N, r_e, r_v, and r_s refers to the adiabatic value.

Furthermore, Eqs. (2) and (9)–(11) can be used to derive LWP and the optical thickness of an adiabatic cloud column, by integration from the cloud base to the cloud top (Boers and Mitchell 1994):

$$W_{ad} = (1/2) C_w H^2, \tag{12}$$

$$\tau_{ad} = (3/5)\pi Q_{ext} A^{2/3} (kN_{ad})^{1/3} H^{5/3}. \tag{13}$$

As discussed above, if all kinds of profiles of $w(h)$ and $r_e(h)$ were possible, there would be no way to relate the optical thickness [$\propto \int_0^H w(h)/r_e(h)\, dh$] to the integrated values of these two parameters separately. The problem is currently solved by assuming that r_e is constant with altitude, but this raises the question on how to define the equivalent VU-PPM effective radius $\langle r_e \rangle$. The adiabatic model provides a more realistic solution to that problem. It also establishes a connection between the optical thickness and a set of two physical parameters of crucial importance for studies of the indirect effect and cloud feedback: H and N. In addition, the coefficient k, which represents the effect of droplet spectral shape on radiation, can be implicitly accounted for by replacing the total droplet concentration N by a scaled droplet concentration kN. Since k is between 0.7 and 1, its effect is not decisive with respect to the expected change in droplet concentration due to an increase in CCN concentration, namely, a factor of 2 to 10 in N.

For complete calculations of the radiative transfer, an adiabatic stratified cloud can thus be modeled as a stack of homogeneous layers, the values of the radiative parameters in each layer being derived from Eqs. (3)–(5), with w and r_e given by Eqs. (9)–(11) as functions of the altitude of the layer above the cloud base. This model is referred to as the AS-PPM.

d. Radiative properties of the subadiabatic cloud regions

An actual convective parcel is open and subject to mixing with the environmental dryer air. Therefore, the actual values of w are smaller or equal to w_{ad}. The observations analyzed in the next section aim at showing that the AS-PPM is more realistic than a VU-PPM, but it must be emphasized that adiabaticity represents a maximum reference for the actual cloud microphysics at all levels. Cloud regions with an LWC close to the adiabatic value (within the range of uncertainty in the evaluation of w, i.e., $\pm 15\%$) will be referred to as quasi-adiabatic regions. Cloud volumes with w significantly lower than w_{ad}, hereafter referred to as subadiabatic volumes, are frequent in a cloud layer. The resulting vertical profiles are, however, difficult to characterize. The main process leading to subadiabaticity is the mixing of the cloudy air with dry air from above the inversion layer. The mixed parcels are then likely to sink into the cloud layer driven by negative buoyancy due to evaporation of cloud droplets. A cloud column can thus appear to be quasi-adiabatic in its lower part and subadiabatic in its upper part. The variety of possible vertical profiles is too large for a simple parameterization. Radiative calculations in this paper are thus restricted to AS-PPM. However, further analysis is planned to examine the effects of subadiabaticity via 3D numerical simulations with a cloud-resolving model. In such a model, w is diagnosed in each grid, but the way N and r_v are altered by mixing processes is not explicitly solved. It is thus crucial to analyze subadiabatic volumes in order to determine how LWC is reduced, whether by a reduction in concentration, or in the droplet sizes, or in both concurrently. Such information is needed to establish a link between LWC and the volume extinction in the model's grids.

3. In situ measurements of cloud microphysics

a. The CLOUDYCOLUMN Project within ACE-2

The Aerosol Characterization Experiments promoted by the International Global Atmospheric Chemistry Project are dedicated to the study of the effects of aerosols on climate. ACE-2 (Raes and Bates 1995), mainly supported by the European Union, was conducted from 15 June to 23 July 1997 in the northeast Atlantic, between Portugal, the Azores, and the Canary Islands. In early summer, this region of the ocean is affected by northerly winds and subsidence, producing extended stratocumulus clouds. The origin of the air in the BL is generally from the Atlantic, and the aerosol background is of the marine type; on some occasions there is a contamination by European pollution. The CLOUDYCOLUMN Project in ACE-2 is a closure experiment focused on the aerosol indirect effect. The basic strategy was to sample similar types of clouds (stratocumulus) with different aerosol backgrounds (Brenguier et al. 2000).

Up to five instrumented aircraft were involved in the field project. The MRF-C130 and/or the CIRPAS Pelican were in charge of the characterization of the subcloud layer for turbulent fluxes and the physical, chemical, and nucleating properties of the aerosols. The Météo-France M-IV was equipped for measurements of cloud microphysics and measurements of the physical and nucleating properties of the aerosols (total aerosol below cloud base and interstitial aerosol in cloud). The DLR/AWI-Do-228 was in charge of remote sensing of

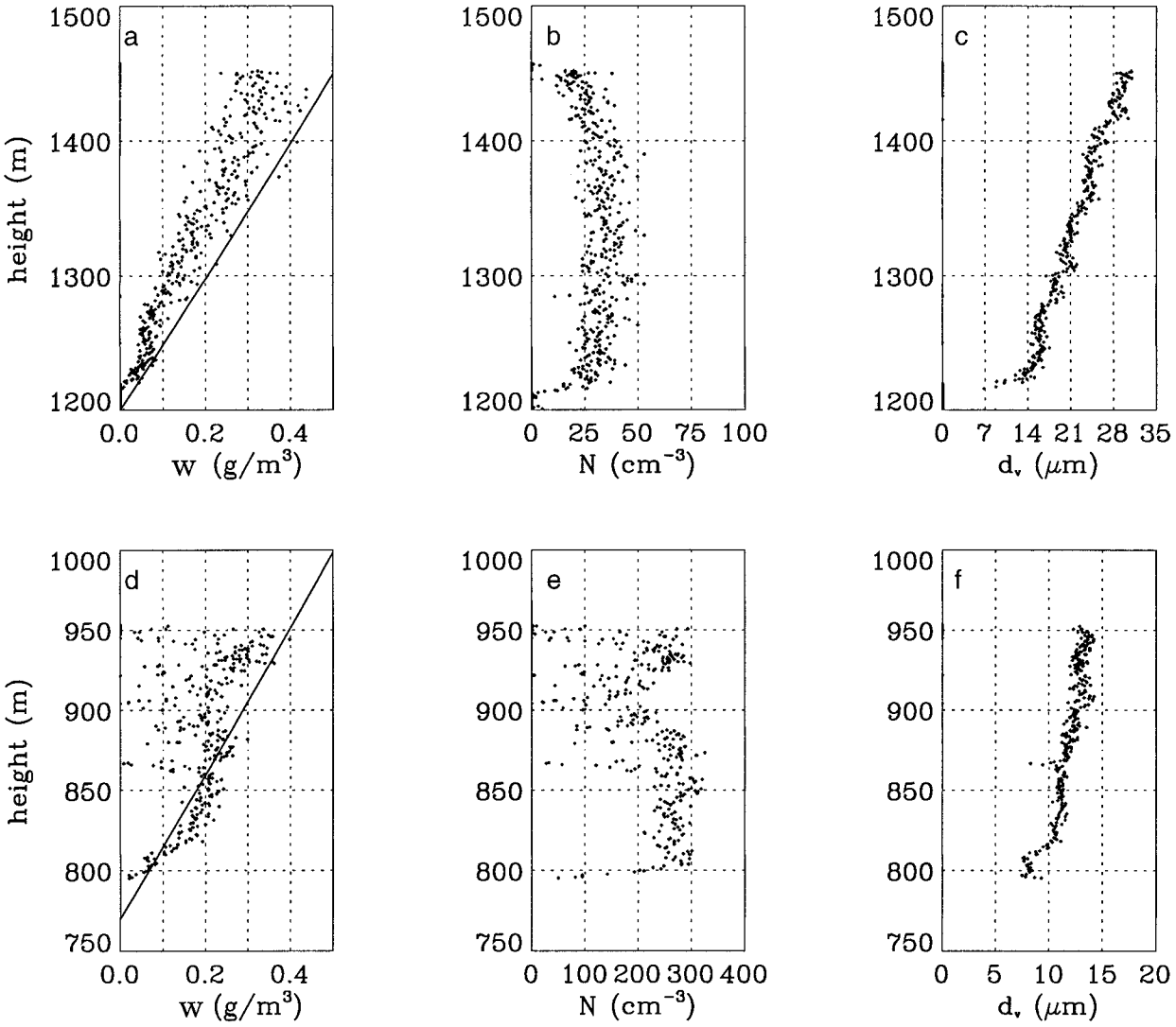

FIG. 1. Examples of vertical profiles of the microphysics measured with the M-IV during an ascent through the cloud layer [26 Jun in (a)–(c) and 9 Jul in (d)–(f) cases]: LWC in (a) and (d), droplet number concentration in (b) and (e), and mean volume diameter in (c) and (f). The solid lines in (a) and (d) represent the adiabatic LWC.

the cloud radiative properties with two radiometers: the POLDER multidirectional radiometer (Descloitres et al. 1995; Parol et al. 2000), and the OVID multispectral radiometer (Schüller et al. 1997; Schüller et al. 2000). The Do-228 flew at 3000 ft above the cloud layer, and its trajectory was closely synchronized with the M-IV in order to maintain the collocation of in situ and remote sensing measurements with an accuracy of 300 m. Two flights were also coordinated with a fifth aircraft, the ARAT-F27, flying 4000 ft above the cloud layer, and equipped with a downward looking lidar (Pelon et al. 1992; Pelon et al. 2000). The flight figures flown concomitantly by the M-IV in the cloud layer and by the Do-228, 3000 ft above, were either 60-km squares with a diagonal oriented toward the solar azimuth (nine flights) or 160-km-long legs oriented also toward the solar azimuth and flown back and forth (two flights).

The measurements of cloud radiative properties discussed in this paper have been performed with the OVID radiometer. The characterization of the cloud vertical profiles of microphysics is based on series of ascents and descents through the cloud layer with the M-IV (see Fig. 1 in Brenguier et al. 2000). There are at least 15, and up to 35, such traverses available per flight (35 profiles on 26 June 1997 and 28 profiles on 9 July 1997). The measurements of the droplet size distributions on board the M-IV were performed with the Fast-FSSP, an improved version of the standard Forward Scattering Spectrometer Probe (Brenguier et al. 1998). Detailed information about the microphysical properties ob-

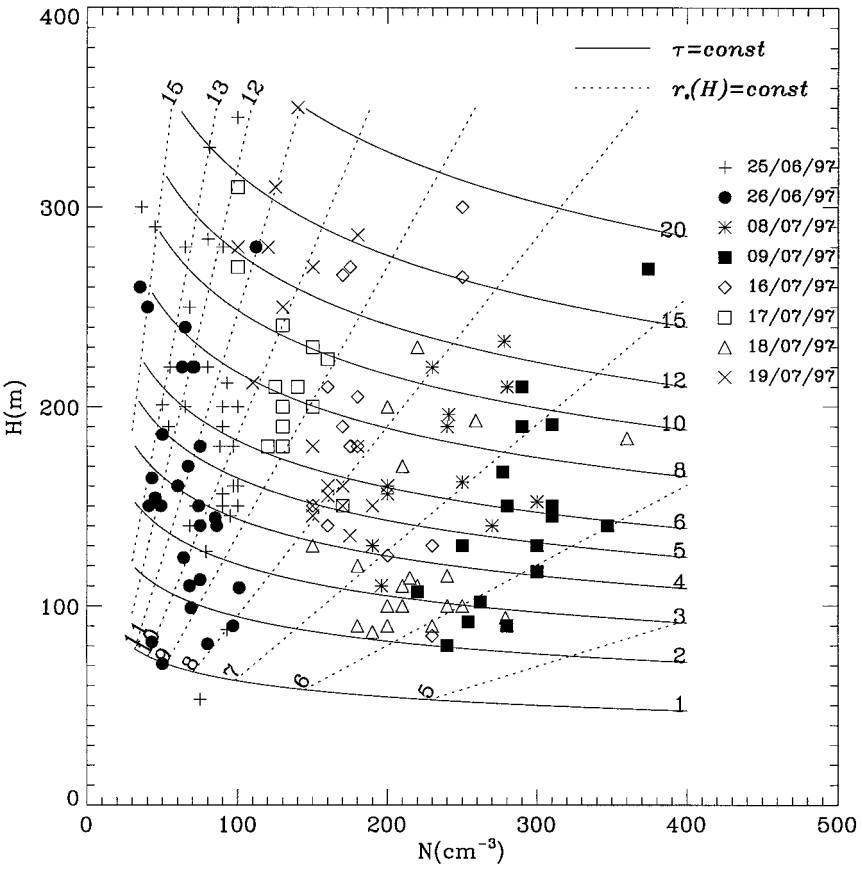

FIG. 2. Typical values of cloud geometrical thicknesses and droplet number concentrations measured along the cloud traverses made during eight flights of the ACE-2 campaign. Each dot corresponds to values derived from in situ measurements with the M-IV during an ascent or descent through the cloud layer. The superimposed isolines are the effective radius at the top of an AS-PPM and the optical thickness, for the corresponding geometrical thickness and droplet number concentration.

served during eight flights of the project can be found in Pawlowska and Brenguier (2000).

b. Vertical profiles

A cloud traverse through the cloud layer with the M-IV, ascending or descending at 1000 ft min^{-1}, is not precisely a vertical profile since the aircraft travels between 3 and 8 km horizontally during the traverse. Figure 1 shows two examples of vertical profiles of the microphysical parameters such as measured along an ascent or descent of the M-IV through the cloud layer, with, successively, the LWC (Figs. 1a,d), the droplet number concentration N (Figs. 1b,e), and the mean volume diameter $d_v = 2r_v$ (Figs. 1c,f). The slope of the adiabatic profile of LWC is indicated in Figs. 1a,d by a solid line. Each dot corresponds to measurements averaged over 0.1 s (≈10-m horizontal distance) in order to better capture the spatial variability of the microphysical fields. Because of the horizontal distance traveled by the aircraft during a cloud traverse, this variability likely reflects horizontal inhomogeneity. Therefore it is necessary to combine many of such traverses in order to obtain a statistically significant description of the cloud layer. In a first step, each traverse is used to estimate the cloud-base and -top altitudes, and thus the cloud geometrical thickness H and the droplet number concentration N for the profile. This N value is derived as the value at 99% of the cumulative frequency distribution of the values measured along the profile.

Figure 2 presents a summary of eight flights. Each dot corresponds to a cloud traverse. The figure shows that two cases were of the pure marine type with $N \leq 110$ cm^{-3} (25 and 26 June). The other cases were partially contaminated by pollution from Europe with N up to 400 cm^{-3} (9 July). The cloud geometrical thickness was always less than 350 m. The isolines in the figure represent the effective radius at the cloud top (dashed curves) and the optical thickness (solid curves) as derived from Eqs. (11) and (13) ($k = 0.8$), respectively, for the corresponding values of H and N. In these equations, the constant A depends slightly on the temperature

in the cloud layer through C_w. The use of a single set of isolines for all the flights, $C_w = 1.9 \times 10^{-3}$ g m^{-4}, is an approximation that is justified by the fact that the temperatures measured over the whole campaign were comparable. These isolines illustrate how the various cases could be classified in terms of optical thickness and effective radius. For example, it can be seen that an effective radius of about 9 μm is representative of either a thin marine cloud ($N = 50$ cm^{-3} and $H = 70$ m) or a thick polluted one ($N = 250$ cm^{-3} and $H = 340$ m). On the contrary, the droplet concentration is a particularly well suited parameter for describing the airmass type.

Two cases in particular will be discussed here: a marine case on 26 June and the most polluted case on 9 July. The advanced very high resolution radiometer images on these two days [see Fig. 3 in Brenguier et al. (2000)] and calculations of the airmass trajectories in the BL confirm that the air mass was originating from the ocean on 26 June and that it was contaminated by European pollution on 9 July.

Figure 1a for 26 June, shows that quasi-adiabatic values of LWC are measured from the cloud base up to the top and that most of the values are greater than 60% of the adiabatic at all levels. On average, w is increasing linearly with altitude at a rate slightly lower than 2×10^{-3} g m^{-4}, which is the value predicted by Eq. (9) for a temperature of 10°C, as measured at cloud base. It is remarkable that the M-IV aircraft remained in a quasi-adiabatic cloud region along the 3.6 km flown while ascending from 1200 to 1450 m. The droplet concentration is smaller than 50 cm^{-3}, a value typical of a marine aerosol background. The rapid increase of N at the cloud base (Fig. 1b) is an instrumental artifact due to droplets at cloud base that are smaller than the detection threshold of the Fast-FSSP (3 μm in diameter). The decrease of N within the uppermost 50 m illustrates the effect of mixing with the overlaying dry air, which progresses from the top on, down within the cloud. However, it is interesting to note that despite the dilution of the droplet concentration, the mean volume diameter (Fig. 1c) does not seem to be affected by the mixing. This crucial feature will be discussed in section 3c.

The second example, for the polluted case on 9 July, shows droplet concentrations larger than 300 cm^{-3} (Fig. 1e). It is representative of an ascent during which the M-IV flew through different cells separated by diluted regions. It confirms the above statement that the droplet sizes are almost not affected by the mixing and the dilution of the droplet concentration.

Figure 3 summarizes the statistical analysis of all the vertical profiles conducted on these two case study days. Figures 3a and 3b show the frequency distributions of w/w_{ad} for 26 June and 9 July. Only values measured above 0.1 H have been considered because at lower levels the uncertainty in the cloud-base altitude estimation introduces large errors in the estimation of w_{ad}. Values larger than 1 reflect the uncertainty in the evaluation of the ratio. Similar observations have been reported from the JASIN experiment by Slingo et al. (1982), and from the EUCREX-94 experiment by Pawlowska and Brenguier (1996). The isocontours of frequency distributions of N and d_v, versus altitude above cloud base, are plotted, respectively, in Figs. 3c and 3e for 26 June, and in Figs. 3d and 3f for 9 July. Finally, the scatterplot of k is shown in Figs. 3g and 3h for the two cases, respectively. Figures 3a,c,e,g include 4770 values, that is, a distance of 48 km in clouds. Figures 3b,d,f,h include 3900 values, that is, a distance of 39 km in clouds.

The marine case is characterized by a slightly thicker cloud layer. The maximum of N at 80 m above cloud base, with a significant decrease above, suggests that entrainment was active in the upper part of the cloud layer. In Figs. 3e,f the vertical profile of the adiabatic mean volume diameter $d_{v\text{ad}} = 2\, r_{v\text{ad}}$ is represented by a solid line, as predicted by Eq. (10), with a droplet number concentration of $N_{\text{mean}} = 54$ m^{-3} for the marine case (Fig. 3e) and $N_{\text{mean}} = 245$ m^{-3} for the polluted case (Fig. 3f). The N_{mean} characterizes the whole flight. It is calculated as the mean value of the N frequency distribution, over all the cloud traverses of the flight, after rejection of samples with a drizzle concentration larger than 2 cm^{-3} and $w < 0.9\, w_{\text{ad}}$ (Pawlowska and Brenguier 2000). These figures demonstrate that droplets are growing according to the adiabatic model so that the mean volume diameter and the effective diameter at the cloud top are dependent upon the cloud geometrical thickness. The measured values of the k coefficient (Figs. 3g,h) confirm previous estimates made by Martin et al. (1994), with values in the marine case slightly larger than in the polluted case. This feature is discussed in detail in Pawlowska and Brenguier (2000).

c. Microphysical properties of subadiabatic regions

From Eq. (1), the adiabatic model [$w(h) = w_{\text{ad}}(h)$ and $N = \text{const}$] provides a simple relationship between $w(h)$ and $d_v(h)$. In an actual cloud, N and d_v are not strictly equal to their adiabatic values for two reasons. (i) The activation process at the cloud base is not unique. Variations of the vertical velocity at the base result in variations of the number of activated nuclei, that is, variations of the droplet number concentration farther up in the cloud. (ii) Dry air is entrained from the cloud top and leads to dilution of the droplets and possibly some evaporation. The key question for the cloud radiative properties is to characterize the statistical distribution of w with respect to the adiabatic value, and also, for a fixed value of w, to determine how the water is distributed among the droplets. For the same LWC, a volume filled with numerous small droplets has a larger extinction than a volume filled with a few large droplets [Eq. (3)]. These properties are synthesized in Fig. 4, for all the cloud samples shown in Fig. 3. First the same N_{mean} value as in the previous section is used as a ref-

erence for the whole flight. Each sample is described by two coordinates: the ratio of the measured N to the reference value N_{mean} and the ratio of the measured d_v^3 to the adiabatic one d_{vad}^3. The latter is derived using Eq. (10) with $w_{\text{ad}}(h)$, calculated for each sample depending on its altitude above cloud base, and $N_{\text{ad}} = N_{\text{mean}}$. The product of the coordinates is thus equal to w/w_{ad}, whose values are illustrated in the figures by isolines from 100% down to 10%. The frequency distribution of the data is represented by colored contours with a scale indicating the percentage of data points inside each contour. In Fig. 4a, there are no values of N/N_{ad} smaller than 1/3 that correspond to the minimum concentration (20 cm^{-3}) needed for a significant calculation of d_v from the droplet spectrum. The values above 100% of w_{ad} illustrate the uncertainty in the estimation of the cloud-base level.

The variability of the droplet concentration in adiabatic cloud volumes for the marine case is revealed by the dispersion of the measured values along the 100% LWC isoline, from 0.5 to 1.6 of the reference value, that is, from 30 to 85 cm^{-3}. This feature illustrates the effect of variable activation at cloud base with regions of higher concentration and smaller sizes, and vice versa. This is common to most of the CLOUDYCOLUMN flights (Pawlowska and Brenguier 2000). The variability seems to be slightly lower in the polluted case, from 0.5 to 1.3 of the reference value. However, the reference being larger than in the marine case, such a relative variation corresponds, in fact, to a variability in droplet concentration from 120 to 320 cm^{-3}. The most interesting peculiarity in Fig. 4b is the fact that low values of w/w_{ad} are due to a decrease in N rather than in d_v^3. This feature suggests that mixing with clear air occurs after the clear air has been moistened by earlier mixing, so that dilution is more significant than evaporation (Baker et al. 1980). The same characteristic is not observable in Fig. 4a because of the processing threshold at $N/N_{\text{ad}} = 1/3$. This important feature of the mixing process has been pointed out by Blyth and Latham (1991) in various types of nonprecipitating clouds such as cumulus in Montana, New Mexico, and Hawaii. It implies that the radiative parameters in a subadiabatic cloud volume at an altitude h above cloud base can be approximated by using

$$r_v(h) = r_{\text{vad}}(h) \tag{14}$$

$$N = N_{\text{ad}} w/w_{\text{ad}}. \tag{15}$$

These formulas provide a realistic parameterization for deriving cloud extinction in the grids of a cloud-resolving model, when only w is diagnosed.

4. Experimental validation of the adiabatic model

It has been shown in the previous section that the adiabatic model provides a more realistic description of the vertical profiles of microphysics than a vertically uniform model. For validation of the use of the AS-PPM for radiative transfer calculation, it is also necessary to evaluate the consequences of such a hypothesis. The main difference between the two models is that the optical thickness is proportional to $H^{5/3}$ in the adiabatic model, while it is only proportional to H in the VU-PPM. This feature is now tested by comparing colocated measurements of cloud microphysics and cloud optical thickness. The validation is based on cloud sections that have been sampled by the M-IV, with the Do-228 measuring spectral radiances at the same location. The H and N, as derived from each ascent or descent through the cloud layer, are used to calculate τ_{ad} with Eq. (13) [$Q_{\text{ext}} = 2$ and C_w derived from the measured temperature at cloud base, according to Brenguier (1991)]. Figure 5 shows the comparison with the values derived from OVID along a leg flown on 25 June directly from the northern corner to the southern corner of the square figure. The retrieval of the optical thickness with OVID is based on an inversion technique using measurements of radiances at two wavelengths (754 and 1535 nm). The method will be discussed further in section 6. The values of optical thickness are drawn as a function of latitude along the leg. Values of τ_{ad} are superimposed with segments corresponding to the horizontal length of the ascent or descent. This figure shows an example of the concordance between the remotely sensed optical thickness and the values derived from in situ measurements. Figure 6a shows, for the 126 cloud sections selected within the eight flights of Fig. 2, the optical thickness derived from OVID and normalized by $A^*N^{1/3}$ [$A^* = (3/5)\pi Q_{\text{ext}} A^{2/3}$] versus $H^{5/3}$, where N and H are the values derived from each cloud traverse. The figure demonstrates that the cloud optical thickness is proportional to $H^{5/3}$ rather than to H. Figure 6b is similar to 6a except that τ is now normalized by $A^*H^{5/3}$ and plotted versus $N^{1/3}$. The proportionality would validate experimentally the concept of aerosol indirect effect. The figure shows the expected trend, but the results are affected by small errors in H and there is a significant scatter. Further analysis of the cloud geometrical thickness based on lidar sampling will soon improve this result.

The linear approximation for the vertical increase of w_{ad} has been often used in parameterizations of the cloud radiative properties (Nakajima and King 1990; Boers and Mitchell 1994; Jones et al. 1994; Pincus and Baker 1994; Pontikis 1996). However, only Boers and Mitchell (1994) pointed out the main inference of the hypothesis, namely, that the optical thickness of clouds is dependent on $H^{5/3}$, which is much larger than the $\tau \propto H$ found by Twomey (1977) and subsequently used in Twomey (1991), Platnick and Twomey (1994), and Baker (1997). This dependence has been clearly demonstrated with the ACE-2 data. A sensitivity of τ to H much stronger ($H^{5/3}$) than its sensitivity to N ($N^{1/3}$) implies that the straight link between N and the albedo could not be the most efficient contribution to the indirect effect. Feedback

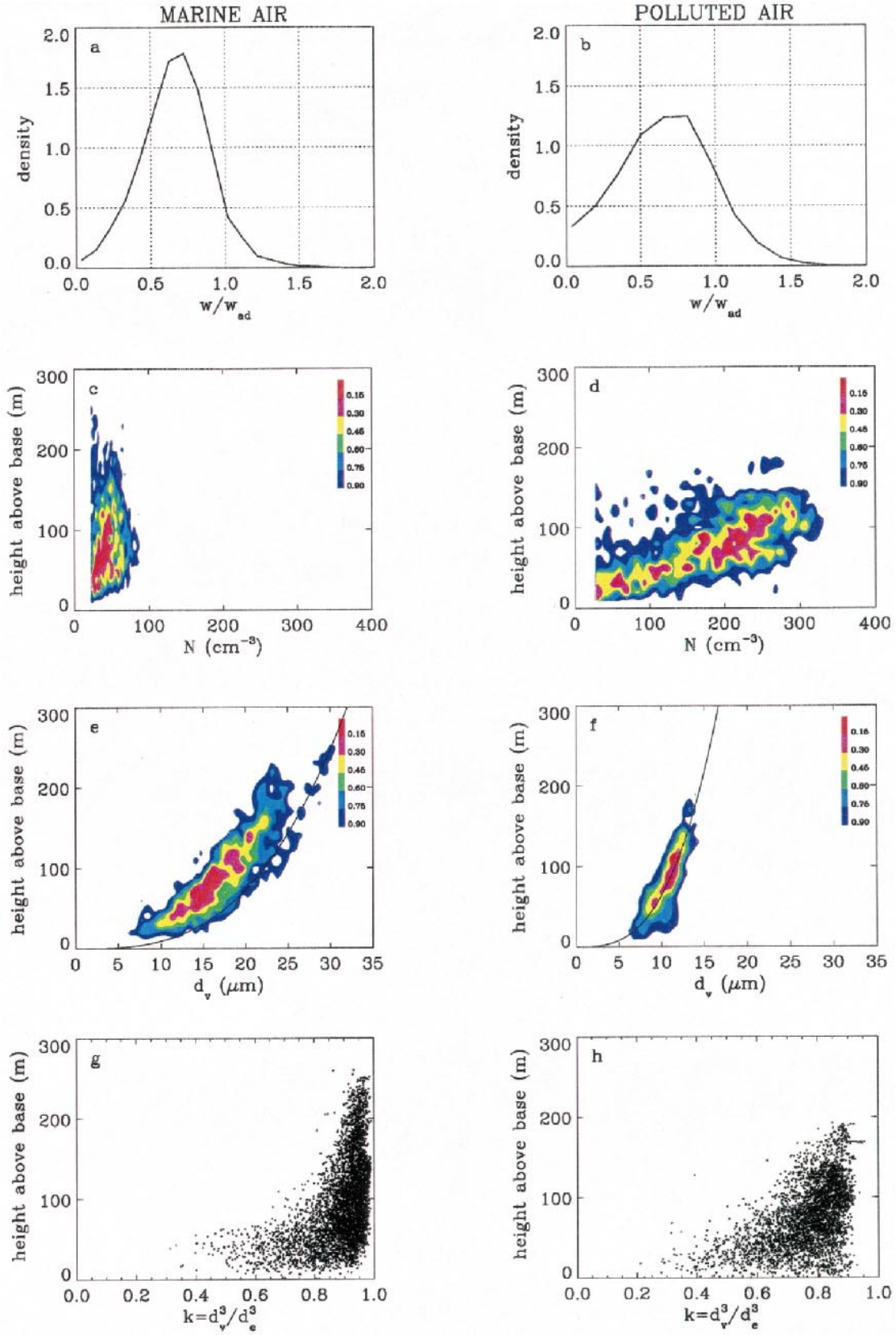

processes such as described by Albrecht (1989), Boers and Mitchell (1994), Pincus and Baker (1994), and Martin et al. (1997) are likely to modify the cloud liquid water path and lead to stronger effects than the direct link between droplet concentration and albedo. In fact, Eq. (13) implies that the effect of doubling the droplet number concentration is comparable to the effect of increasing the cloud geometrical thickness by only 15%.

5. The possible equivalence between the VU-PPM and the AS-PPM

The simplicity of the VU-PPM is attractive for solving the radiative transfer through a cloud. It is thus relevant to investigate the possible equivalence between the VU-PPM and the AS-PPM. The W and τ are vertically integrated parameters, while r_e is not. The first step is to determine with a radiative transfer model a relationship between the VU-PPM equivalent effective radius $\langle r_e \rangle$ and a specific value of the AS-PPM. The optical thickness in a VU-PPM can be expressed as

$$\langle \tau \rangle = \langle \sigma_{\text{ext}} \rangle H = \frac{3Q_{\text{ext}}}{4\rho_w} \frac{\langle w \rangle H}{\langle r_e \rangle} = \frac{3Q_{\text{ext}}}{4\rho_w} \frac{\langle W \rangle}{\langle r_e \rangle}, \quad (16)$$

where $\langle w \rangle$ is constant with altitude. From $\langle W \rangle = W_{\text{ad}}$, $\langle \tau \rangle = \tau_{\text{ad}}$, and using Eqs. (2) and (13), it results that $\langle r_e \rangle = (5/6) r_e(H)$. The second step is to investigate the equivalence of the two models. This was evaluated by examining the reflectance at two wavelengths: 754 and 1535 nm. The calculations were performed with the Matrix Operator Model (MOMO), a radiative transfer model (Fischer and Grassl 1991) based on the Matrix Operator Method (Plass et al. 1973). This technique is similar to the adding–doubling method mentioned above. The scattering and absorption coefficients and the corresponding phase functions of aerosols and cloud particles are obtained with the Mie theory. A modified-gamma drop size distribution (Hansen and Travis 1974) is used in the calculations. The reflectance values shown in the following figures are for a solar zenith angle of $\theta_s = 30°$.

Initially, 48 samples of (N, H) are selected with $25 \leq N \leq 800$ cm^{-3} and $200 \leq H \leq 1000$ m. The stratified model is simulated as a stack of 25-m-thick layers (from 8 layers at $H = 200$ m to 40 layers at $H = 1000$ m). The values of $w_{\text{ad}}(h)$ and $r_{e\text{ad}}(h)$ are then calculated at the middle of each layer with Eqs. (9) and (11), with $k = 0.75$; and the corresponding $\sigma_{\text{ext},i}$, ω_i, and g_i are derived with Eqs. (3)–(5), for $\lambda = 754$ nm and $\lambda = 1535$ nm. The MOMO model applied to this multilayer cloud provides the reflectances at the two selected wavelengths. The same model is then used with a single-layer VU-PPM cloud in order to retrieve the values of $\langle \tau \rangle$ and $\langle r_e \rangle$ that are producing the same reflectances as the multilayer model at the two wavelengths.

Figure 7a shows the comparison of $\langle \tau \rangle$ with the optical thickness of the multilayered cloud calculated as the sum of the extinctions in each layer ($\times 25$ m). The two values are comparable for the whole sample set, up to optical thicknesses of more than 80. The slight discrepancies can be attributed to the discretization of H and to numerical errors. Figure 7b shows the comparison of $\langle r_e \rangle$ with 5/6 of the effective radius at the top of the multilayer cloud, as implied by the equivalence of W and τ.

Except for two specific values ($\langle r_e \rangle \approx 5$ μm and $\langle r_e \rangle \approx 18$ μm), at which some agreement occurs between the VU-PPM effective radius and the expected value of $(5/6) r_e(H)$, there is a significant dispersion apart from the expected 5/6 slope. The difference reaches up to 2.5 μm at $\langle r_e \rangle \approx 13$ μm. In general, the value of the effective radius to use in the VU-PPM is larger than 5/6 of the effective radius at the top of the AS-PPM. The 6/5 slope in Fig. 7b shows that in the worst case, the VU-PPM effective radius is equal to the effective radius at the top of the AS-PPM. This feature could explain the variety of solutions that have been proposed in the literature, as discussed in section 2b. It can be concluded from this test that there is no constant proportionality between the effective radius to use in a VU-PPM and the effective radius at the top of the AS-PPM, though the coefficient of proportionality might possibly be calculated as a function of N and H.

6. Retrieval of cloud parameters from remote sensing

The implementation and validation of an AS-PPM based parameterization in a GCM is a long task, but its efficiency can be directly tested on the techniques developed for the retrieval of cloud properties from remote sensing of multispectral cloud radiances. The test performed in the previous section was derived from techniques that have been developed for the retrieval of τ and r_e from satellite measurements of cloud reflectances in the visible and near infrared (Twomey and Cocks 1989; Nakajima and King 1990; Han et al. 1994; Platnick and Valero 1995). VU-PPM models were run for various values of τ and r_e, and reflectances at the two wavelengths were calculated and stored in tables. The inverse procedure is then applied to derive these parameters from satellite reflectance measurements. Figure 8

←

FIG. 3. Summary of the microphysical data measured during the 26 Jun cases in (a), (c), (e), and (g) and 9 Jul cases in (b), (d), (f), and (h), for all the profiles performed through the cloud layer. (a), (b) Frequency distributions of w/w_{ad}. (c), (d) Isocontours of frequency distribution for the droplet number concentration vs height above cloud base. (e), (f) Same for the mean volume diameter; the solid lines represent the predicted profiles for an adiabatic stratified cloud. (g), (h) Scatterplot of the k coefficient.

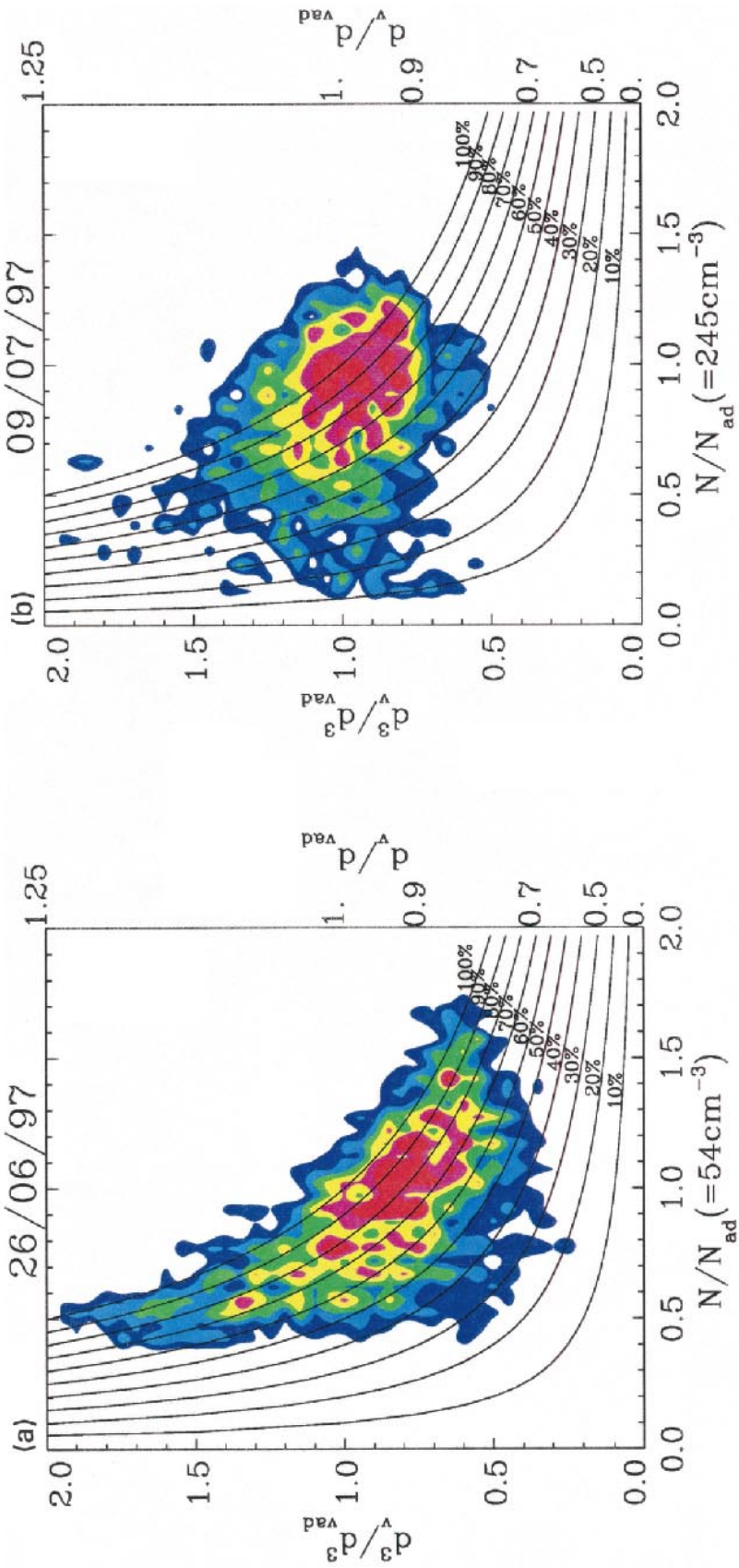

FIG. 4. Frequency distributions of the mean volume diameter vs droplet number concentration for (a) the 26 Jun case and (b) the 9 Jul case. The measured droplet number concentration is normalized by N_{mean}, which has been selected as a reference for the whole cloud layer. The measured value of mean droplet diameter is normalized by the value predicted by the adiabatic model with the same reference value of droplet number concentration, at the corresponding altitude. Isolines correspond to values of the ratio of measured w to the adiabatic one, from 100% to 10%.

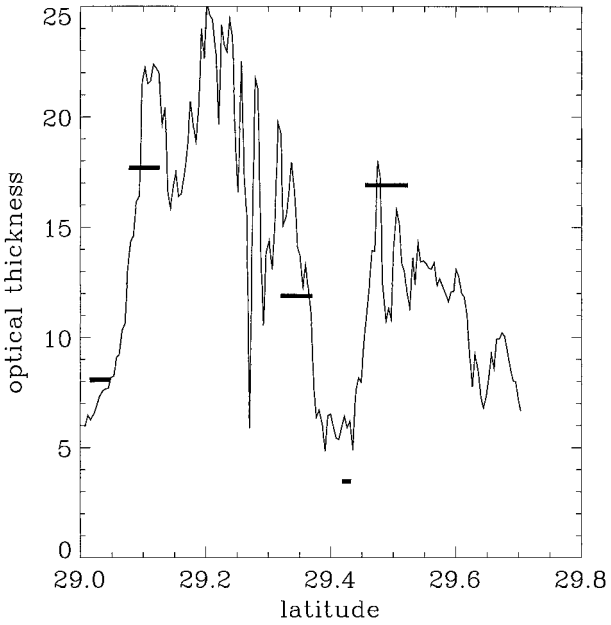

FIG. 5. Comparison of the values of optical thickness derived from in situ measurements during ascents or descents through the cloud layer with the M-IV, with the values derived along the Do-228 track from the OVID measured radiances. The short segments represent the horizontal distance flown by the M-IV during the cloud traverses.

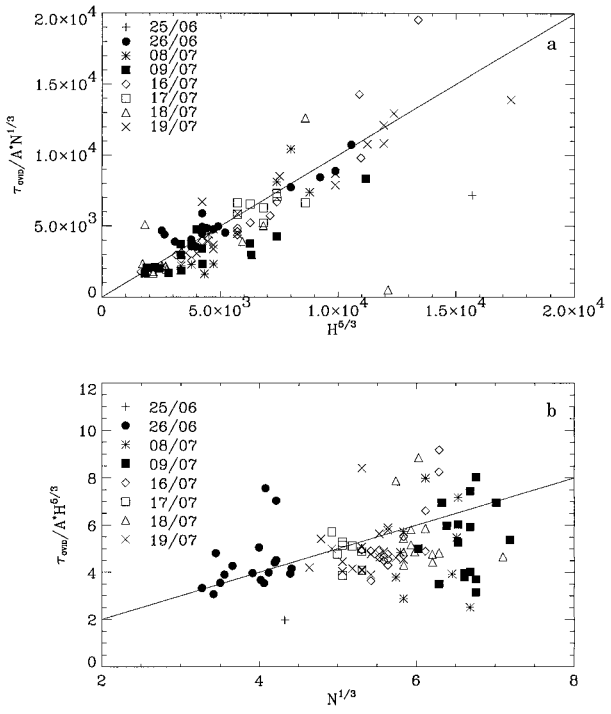

FIG. 6. (a) Optical thickness derived from OVID measurements and normalized by $A^*N^{1/3}$ as function of $H^{5/3}$, where N and H are the values measured in situ. Each dot corresponds to an ascent or descent through the cloud layer with the M-IV, during eight flights of the ACE-2 campaign. (b) Same as (a) with the optical thickness derived from OVID measurements and normalized by $A^*H^{5/3}$ as function of $N^{1/3}$.

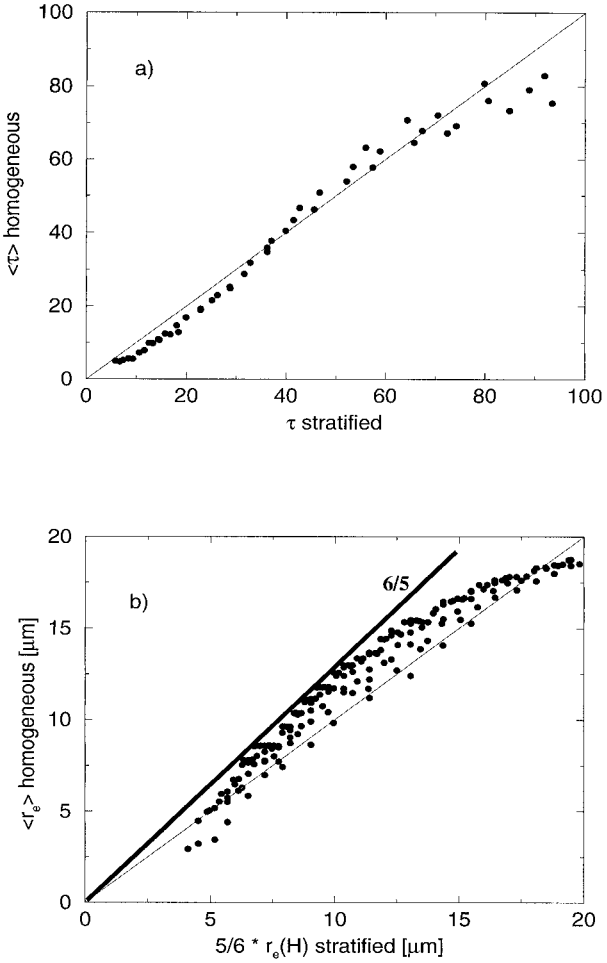

FIG. 7. Comparison of the homogeneous VU-PPM and the AS-PPM for parameterization of radiative transfer in clouds: (a) optical thickness and (b) effective radius. The effective radius of the homogeneous model $\langle r_e \rangle$ is compared to 5/6 of the effective radius at the top of the AS-PPM $r_e(H)$.

illustrates the technique. It shows the conditional frequency distributions of cloud reflectances at 754 versus 1535 nm over the whole flight. These values are derived from airborne measurements of the multispectral radiances with OVID on board the Do-228. Figures 8a and 8c are for the marine case on 26 June, and Figs. 8b and 8d are for the polluted case on 9 July. In Figs. 8a and 8b isolines of τ and r_e have been reproduced. The data cover a large range of optical thicknesses and effective radii, from $\tau = 4$ to 12 and $r_e = 8$ to 14 μm in the marine case, from $\tau = 2$ to 30 and $r_e = 4$ to 10 μm in the polluted case. Nevertheless, the difference between the two distributions is noticeable. It reflects the aerosol indirect effect at the scale of a cloud system. The first observations of the indirect effect were limited to ship tracks (King et al. 1993). They were related to very localized changes in droplet concentration along the tracks. The difference between winter and summer clouds reported by Boers et al. (1998) constitutes a dem-

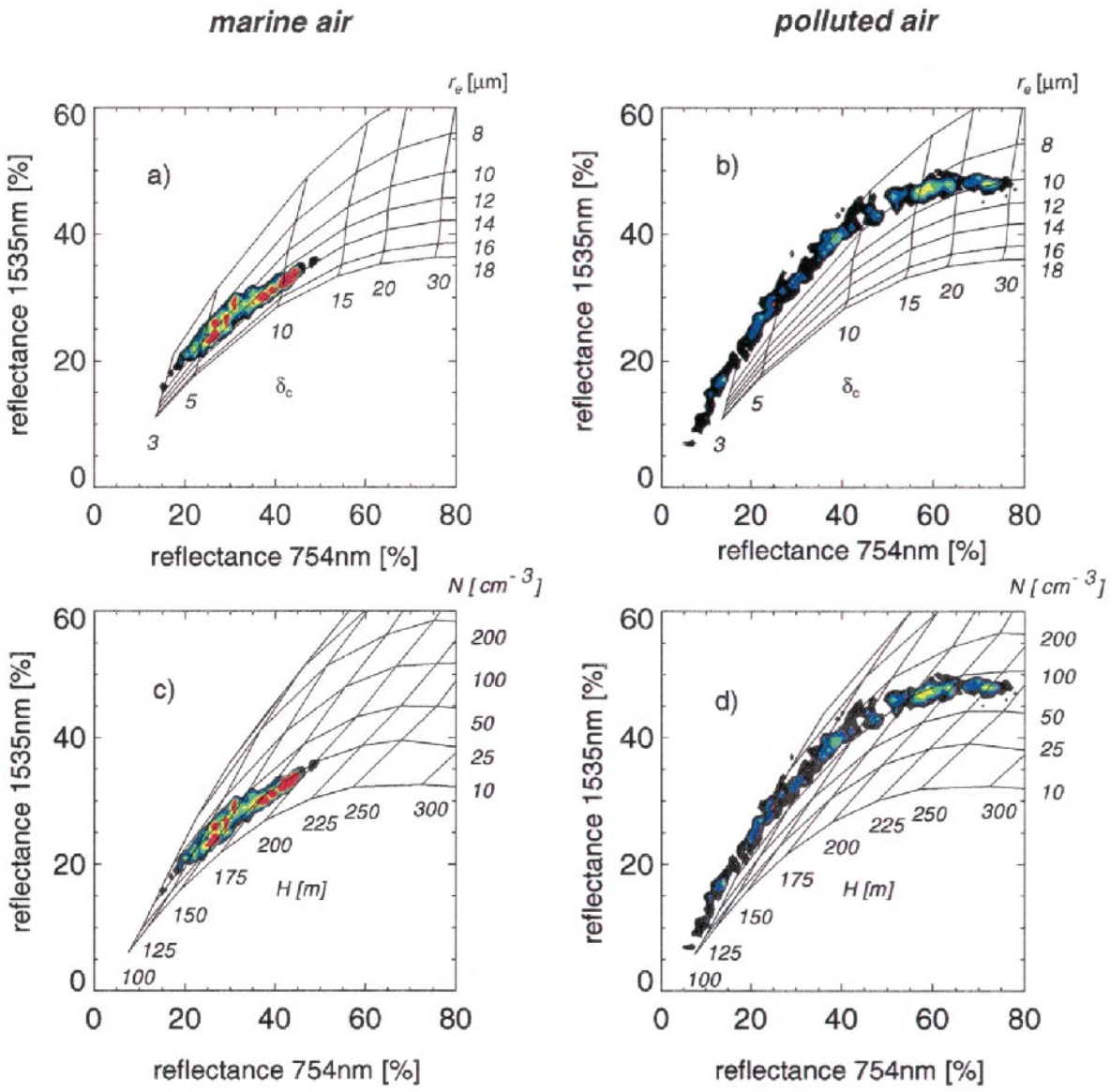

FIG. 8. Frequency distributions of the reflectances at 1535 nm vs reflectances at 754 nm, as derived from OVID measurements for the 26 Jun case in (a) and (c) and the 9 Jul case in (b) and (d); isolines of optical thickness and effective radius predicted by the VU-PPM model in (a) and (b); isolines of geometrical thickness and droplet number concentration predicted by the AS-PPM in (c) and (d).

onstration of changes in cloud radiative properties due to changes in droplet concentration at the scale of a cloud system. The modification of the droplet concentration in this case was related to a natural change in the aerosol properties. The examples shown in Fig. 8 provide a complementary observation of the indirect effect, but associated to anthropogenic pollution from remote sources in Europe.

Despite the significant difference between the two distributions, it is difficult to assign specific values of the effective radius to each case. For the same values of optical thickness, the marine case is characterized by larger radii than the polluted case, but both cases show the same trend, namely, an increase of the effective radius with the optical thickness. This feature reflects the fact that large values of optical thickness are associated with thick clouds (see also Fig. 6a) and therefore large effective radii [Eq. (11)]: a thin marine cloud has the same effective radius at cloud top as a thick polluted cloud, if $H^{5/3}N^{1/3}$ is kept constant. Figures 8c and 8d show the same data, but isolines of τ and r_e have been replaced by isolines of N and H as calculated with the AS-PPM. The orientation of the N isolines is slightly different from the orientation of the r_e isolines, and it becomes feasible to assign specific values of droplet concentration to each case, from 25 to 50 cm^{-3} for the marine case, from 100 to 400 cm^{-3} for the polluted case.

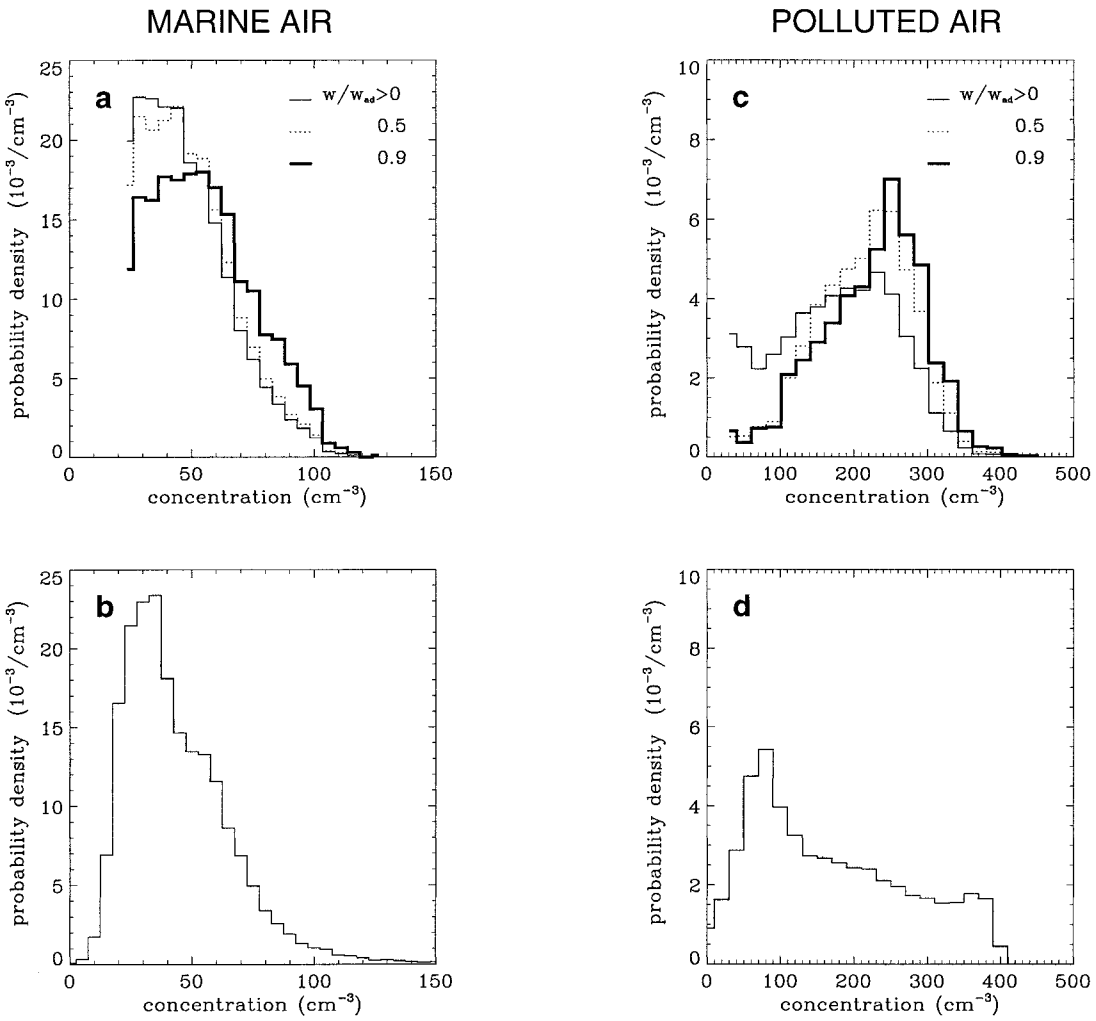

FIG. 9. Frequency distributions of the droplet number concentrations for (a) and (b) the 26 Jun case; and (c) and (d) the 9 Jul case; (a) and (b) measured in situ by the M-IV, with three conditions on the ratio of the corresponding LWC to the adiabatic one; (b) and (c) derived from OVID measurements on the Do-228 in (b) and (d).

The contour plots in Fig. 8 have been drawn with all the values of radiance measured along the aircraft track with OVID, some originating from quasi-adiabatic cloud turrets, others from diluted cloud regions. The quasi-adiabatic regions correspond to the largest values of reflectance. It is remarkable that the values corresponding to subadiabatic cloud regions form the narrow features seen in the figures. That implies that mixing does not produce a large variety of microphysical states and that relationships similar to those derived in adiabatic columns hold for the subadiabatic regions. This result together with the in situ observations described in section 3c will be analyzed for extending the adiabatic parameterization to the subadiabatic cloud volumes.

Figure 9 compares the frequency distributions of the droplet number concentrations measured in situ (Figs. 9a,c) and retrieved from reflectance measurements (Figs. 9b,d) for the marine case (Figs. 9a,b) and the polluted case (Figs. 9c,d). For the values measured in situ three distributions have been plotted: with all the samples (thin solid line), for samples with $0.5 \leq w/w_{ad}$ (dashed line), and samples with $0.9 \leq w/w_{ad}$ (thick solid line). It is obvious that the quasi-adiabatic regions ($0.9 \leq w/w_{ad}$) correspond to the largest values of droplet concentration since subadiabaticity is mainly due to a dilution of the droplet concentration (see Fig. 4). The distributions of concentration derived from remote sensing show also a significant difference between the marine case and the polluted one: most of the marine case values are below 100 cm^{-3}, while values as high as 400 cm^{-3} have been retrieved for the polluted case. However, the frequency distributions are quite different from the measured ones, especially for the polluted case (Figs. 9c,d). The values of the retrieved concentration that are significantly underestimated (the peak at 100 cm^{-3} in Fig. 9d) are, in fact, related to the largest values of the retrieved cloud geometrical thickness, as can be inferred from Fig. 8. This is contradictory to in situ observations,

and it suggests that the discrepancy between retrieved and measured values is not due to subadiabaticity. The bias can also be attributed to an underestimation of the reflectance at 1535 nm, a common feature of radiance measurements, which has been referred to as anomalous absorption by many authors (Twomey and Cocks 1989; Stephens and Tsay 1990; Rawlins and Foot 1990; King et al. 1990). The results presented here suggest that the underestimation increases with the cloud geometrical thickness.

7. Discussion

The CLOUDYCOLUMN Project aims at preparing GCM simulations of the indirect effect and anticipates that the nucleation properties of aerosols will be soon available in these models. The approach is strictly restricted to extended BL clouds with no or little precipitation. The main objective is thus to diagnose the radiative properties of these cloud systems, assuming that the droplet concentration is known.

a. Prediction of the droplet number concentration

In a convective cloud, the droplet number concentration is determined by the nucleation properties of the CCN, by the temperature, and by the intensity of the updraft at the cloud base. Even if the CCN are homogeneously mixed in the BL and if the temperature is uniform at the cloud base, the intensity of the updrafts varies significantly because of the turbulence in the BL. In addition, the values of droplet concentration fixed at the activation level are likely to be modified farther up by entrainment and mixing processes, as well as by drizzle scavenging. Therefore, it is unrealistic to presume that the droplet concentration must be diagnosed with an accuracy of a few percent (Chuang et al. 1997). The microphysical analysis of eight CLOUDYCOLUMN flights (Pawlowska and Brenguier 2000) reveals that the frequency distributions of N in quasi-adiabatic cloud samples extend from 0.5 to 1.5 of the mean value. It is not even necessary to estimate the droplet concentration with a high accuracy because the cloud radiative properties are only sensitive to $N^{1/3}$. The indirect effect becomes a concern, however, because pollution has the capability to increase the natural droplet concentration of marine clouds by a factor of 2 to 10, even far from the sources. We are thus concerned with large changes of the droplet concentration from less than 100 cm^{-3} in a pure marine atmosphere up to 1000 cm^{-3} in a heavily polluted air mass.

b. Parameterization of the indirect effect in GCMs

The observations presented here have demonstrated that cloud radiative properties are particularly sensitive to the cloud geometrical thickness ($H^{5/3}$) and less sensitive to the droplet concentration ($N^{1/3}$). For numerical simulations of the indirect effect and the possible coupling with the cloud geometrical thickness and LWP, it is thus crucial to improve GCM parameterizations. The coefficients a_i to f_i in Eqs. (3)–(5) have been determined with a high accuracy (10^{-3}). The value of the coefficient k [Eq. (11)] that describes the difference between the mean volume radius and the effective radius of a droplet distribution has been empirically estimated at better than 10%, while it affects the derivation of r_e as $k^{1/3}$ only. On the contrary, there is still as much as 30% variability in the way the effective radius is derived from LWC and the droplet concentration in the common VU-PPM. With the AS-PPM, as used in section 5, the values of w and r_e in each layer can be derived from Eqs. (9)–(11). Obviously that does not mean that the radiative properties of a cloud can be calculated to within a few percent since only a limited fraction of the cloud volume exhibits quasi-adiabatic profiles of the microphysics. However, the results presented here indicate that the AS-PPM is more realistic than the VU-PPM for the calculation of the radiative transfer, while the calculations remain as simple as with a VU-PPM. For subadiabatic cloud volumes, the empirical results summarized in Eqs. (14) and (15) can be used as the most realistic approximation. For example, the numerical studies of the effects of horizontal cloud inhomogeneities on albedo are currently based on numerical simulations of inhomogeneous clouds generated either with a cloud-resolving model or with a stochastic model that reproduces the statistical properties of the cloud morphology (Cahalan et al. 1994a,b; 1995). Such models generate inhomogeneous three-dimensional clouds made of a mosaic of homogeneous boxes with variable LWC. Additional information is thus needed for inferring the value of r_e in each grid and deriving the radiative parameters [Eqs. (3)–(5)]. The parameterization proposed here consists of calculating for each altitude above cloud base the values of $r_{ead}(h)$ [Eq. (11)]. The radiative parameters can then be derived in each grid according to Eqs. (14) and (15) as functions of the value of $w(h)$ in the grid and a value of effective radius equal to the predicted value $r_{ead}(h)$ at the grid's altitude level. This scheme is presently tested with our observations.

Climate models provide a prognostic of cloud cover in large grids of the order of 50–100-km sides. With subgrid parameterizations, it is possible to derive morphological parameters such as the cloud geometrical thickness and liquid water path. Aerosol transport models will soon provide estimations of the droplet number concentration. With a radiative scheme based on optical thickness and the effective radius, an additional step would be needed for the simulation of the indirect effect, namely, a relation between cloud morphology and droplet concentration on the one hand, optical thickness and effective radius on the other hand. The effective radius that has been introduced for the calculation of the radiative properties of a cloud volume is not an intrinsic parameter of a cloud as are its geometrical thickness,

optical thickness, liquid water path, and droplet concentration. The droplet concentration characterizes the level of contamination by pollution with values below 100 cm^{-3} in marine air up to values larger than 1000 cm^{-3} in heavily polluted air masses. On the contrary, the effective radius varies in clouds from 0 at the cloud base to a maximum close to cloud top, no matter what the value of the droplet concentration is.

The AS-PPM provides an efficient solution for deriving the vertical profile of r_e from the droplet concentration. It implies, too, that the cloud optical thickness is proportional to $H^{5/3}$. This result suggests that feedback processes that could modify cloud geometrical thickness and LWP shall be considered concurrently with the Twomey effect. In particular, attention must be given to the possible effects of the droplet concentration on precipitation efficiency, since drizzle formation plays an important role in the dissipation of stratocumulus. At the scale of a GCM, the effect of drizzle is a removal of the cloud water, thus reducing LWP. Instead of using N and H as independent variables in the parameterization of cloud optical thickness, Eqs. (9) and (13) can be used to express it as a function of N and W as

$$\tau_{\mathrm{ad}} = (6/5)\pi Q_{\mathrm{ext}} B^{2/3} (kN_{\mathrm{ad}})^{1/3} W^{5/6}, \qquad (17)$$

where $B = [(4/3)\pi\rho_w]^{-1}(2C_w)^{-1/4}$. This formula reveals that it is not necessary to diagnose explicitly the cloud geometrical thickness in a GCM grid, since it is equivalent to diagnosing the LWP. In fact, the constraint of adiabaticity establishes a relationship between the two independent variables currently used in GCM parameterizations of the optical thickness (W and r_e) and either N and W or N and H. It must, however, be emphasized that this relationship is only valid at the scale of a convective cell. It follows that the subgrid parameterization of the cloud fraction in a GCM plays a crucial role in the simulation of the aerosol indirect effect. For the same LWP in a grid, a uniform and thin cloud layer will result in a much greater indirect effect than a few isolated thicker clouds.

c. *Retrieval of droplet concentration and cloud geometrical thickness from remote sensing*

Radiative transfer models are also used for the retrieval of cloud parameters from remote sensing measurements of cloud reflectances. Optical thickness and the effective radius can thus be derived. However, an apparent increase of the effective radius can be attributed to either an increase in the cloud geometrical thickness or a decrease in droplet concentration. With the AS-PPM, reflectances can be directly related to cloud geometrical thickness and droplet concentration. Recently, Rosenfeld and Lensky (1998) have derived, from satellite observations of cumulus cloud fields, distributions of r_e at cloud top as a function of the cloud-top temperature. The resulting distributions can be interpreted as vertical profiles of r_e, and the use of the AS-PPM could be useful for the retrieval of the droplet concentration and therefore the level of contamination of the air mass.

The remote sensing measurements performed with the OVID airborne multispectral radiometer during ACE-2 have validated the technique. Despite a significant underestimation of the retrieved values of droplet concentration, they show evidence of the indirect effect at the scale of a cloud system (Fig. 8).

8. Conclusions

In situ measurements of microphysical parameters in stratocumulus have been performed in synchronization with remote sensing measurements of cloud reflectance. Clouds of similar thicknesses (lower than 350 m) have been sampled in air masses of different origins. Marine cases are characterized by droplet concentrations lower than 100 cm^{-3}, while polluted air masses show concentrations up to 400 cm^{-3}. These measurements confirm previous observations in similar clouds, showing quasi-adiabatic profiles of LWC and mean volume diameter. Estimations of the cloud optical thickness based on the adiabatic model have been derived for a large number of cloud samples. Each sample is characterized by the values of cloud geometrical thickness H and droplet number concentration N measured in situ. These estimations have been compared to the values derived from remote sensing at the same locations. They validate the adiabatic model and confirm that the cloud optical thickness is proportional to $H^{5/3}$. These results also show that optical thickness is proportional to $N^{1/3}$, which is the basis of the indirect effect.

The vertically uniform plane-parallel model (VU-PPM) calculations for various values of H and N have been compared to more detailed calculations performed with an adiabatic stratified plane-parallel model (AS-PPM). The comparison shows that the value of the effective radius to use in a VU-PPM is between 80% and 100% of the value at the top of the AS-PPM. The analysis of the difference between the $\langle r_e \rangle$ and $(5/6)r_e(H)$ suggests that the residual uncertainty depends on H and N. We also used the AS-PPM to calculate tables of reflectances for various values of H and N. These tables allow the retrieval of these two parameters from radiance measurements performed at two wavelengths in the visible and near infrared. Also analyzed are the droplet concentration frequency distributions, corresponding both to values derived from radiance measurements and from the in situ observations. The retrieved values are significantly underestimated, but the difference between the marine case and the polluted one is clearly identified. This observation provides a demonstration of the aerosol indirect effect at the scale of a cloud system, related to anthropogenic pollution.

For GCM parameterizations of the aerosol indirect effect, the adiabatic model provides a relationship between the droplet concentration, which characterizes the

contamination of the air mass, and the cloud optical properties. The results presented here suggest that a very high accuracy in the prediction of the droplet concentration is not required for the following reasons: (i) this parameter is naturally highly variable in clouds, from 0.5 to 1.5 of its mean value; (ii) the indirect effect is sensitive to the cube root of N; and (iii) the expected change in number concentration due to pollution is a factor of 2 to 10. Furthermore we have demonstrated that cloud radiative properties are particularly sensitive to the cloud geometrical thickness and liquid water path. Therefore, the subgrid parameterization of either the liquid water path or the cloud geometrical thickness, and the parameterization of the precipitation efficiency, are crucial steps for improving the simulation of the aerosol indirect effect.

This preliminary analysis of the ACE-2 dataset is encouraging. There is already a good correspondence between the cloud radiative properties derived from in situ measurements and those derived from remote sensing measurements, at the scale of individual cloud cells. Additional analysis is required to better understand the discrepancy between the values of concentration measured in situ and the values derived from remote sensing of cloud radiances. In particular, the role of the subadiabaticity on cloud optical properties must be precisely evaluated. Future work will thus extend the present analysis to larger scales and produce comparisons to satellite remote sensing of cloud albedo at the scale of a cloud system.

Acknowledgments. The authors acknowledge the contributions of the ACE-2 participants, and particularly the aircraft teams from DLR and Météo-France for conducting the flights. They are particularly grateful to C. Martin R. Platt for his very constructive comments that significantly improved the manuscript. This work has been supported by Météo-France, INSU, and the European Union under Grant ENV4-CT95-0117.

REFERENCES

Ackerman, A. S., O. B. Toon, and P. V. Hobbs, 1993: Dissipation of marine stratiform clouds and collapse of the marine boundary layer due to the depletion of cloud condensation nuclei by clouds. *Science,* **262,** 226–229.

Albrecht, B. A., 1989: Aerosols, cloud microphysics, and fractional cloudiness. *Science,* **245,** 1227–1230.

Arking, A., 1991: The radiative effects of clouds and their impact on climate. *Bull. Amer. Meteor. Soc.,* **72,** 795–813.

Baker, M. B., 1997: Cloud microphysics and climate. *Science,* **276,** 1072–1078.

——, R. G. Corbin, and J. Latham, 1980: The influence of entrainment on the evolution of cloud-droplet spectra: I. A model of inhomogeneous mixing. *Quart. J. Roy. Meteor. Soc.,* **106,** 581–598.

Barker, H. W., 1992: Solar radiative transfer through clouds possessing isotropic variable extinction coefficient. *Quart. J. Roy. Meteor. Soc.,* **118,** 1145–1162.

——, 1996: Estimating cloud field albedo using one-dimensional series of optical depth. *J. Atmos. Sci.,* **53,** 2826–2837.

Blyth, A. M., and J. Latham, 1991: A climatological parameterization for cumulus clouds. *J. Atmos. Sci.,* **48,** 2367–2371.

Boers, R., and R. M. Mitchell, 1994: Absorption feedback in stratocumulus clouds: Influence on cloud top albedo. *Tellus,* **46A,** 229–241.

——, J. B. Jensen, and P. B. Krummel, 1998: Microphysical and short-wave radiative structure of stratocumulus clouds over the Southern Ocean: Summer results and seasonal differences. *Quart. J. Roy. Meteor. Soc.,* **124,** 151–168.

Bower, K. N., and T. W. Choularton, 1992: A parameterization of the effective radius of ice free clouds for use in global climate models. *Atmos. Res.,* **27,** 305–339.

Brenguier, J. L., 1991: Parameterization of the condensation process: A theoretical approach. *J. Atmos. Sci.,* **48,** 264–282.

——, T. Bourrianne, A. de Araujo Coelho, J. Isbert, R. Peytavi, D. Trevarin, and P. Weschler, 1998: Improvements of droplet size distribution measurements with the Fast-FSSP (Forward Scattering Spectrometer Probe). *J. Atmos. Oceanic Technol.,* **15,** 1077–1090.

——, and Coauthors, 2000: An overview of the ACE-2 CLOUDY-COLUMN Closure Experiment. *Tellus,* in press.

Cahalan, R. F., W. Ridgway, J. W. Wiscombe, and T. L. Bell, 1994a: The albedo of fractal stratocumulus clouds. *J. Atmos. Sci.,* **51,** 2434–2455.

——, ——, and ——, 1994b: Independent pixel and Monte Carlo estimates of stratocumulus albedo. *J. Atmos. Sci.,* **51,** 3776–3790.

——, D. Silberstein, and J. B. Snider, 1995: Liquid water path and plane-parallel albedo bias during ASTEX. *J. Atmos. Sci.,* **52,** 3002–3012.

Charlson, R. J., J. E. Lovelock, M. O. Andreae, and S. G. Warren, 1987: Oceanic phytoplankton, atmospheric sulphur, cloud albedo and climate. *Nature,* **326,** 655–661.

Chuang, P. Y., R. J. Charlson, and J. H. Seinfeld, 1997: Kinetic limitations on droplet formation in clouds. *Nature,* **390,** 594–596.

Coakley, J. A., Jr., and P. Chýlek, 1975: The two-stream approximation in radiative transfer: Including the angle of the incident radiation. *J. Atmos. Sci.,* **32,** 409–418.

Davis, A., A. Marshak, J. W. Wiscombe, and R. Cahalan, 1996: Scale invariance of liquid water distributions in marine stratocumulus. Part I: Spectral properties and stationarity issues. *J. Atmos. Sci.,* **53,** 1538–1558.

Del Genio, A. D., M. S. Yao, W. Kovari, and K. K. W. Lo, 1996: A prognostic cloud water parameterization for global climate models. *J. Climate,* **9,** 270–304.

Descloitres, I., F. Parol, and J. C. Buriez, 1995: On the validity of the plane-parallel approximation for cloud reflectances as measured from POLDER during ASTEX. *Ann. Geophys.,* **13,** 108–110.

Duda, D. P., G. L. Stephens, B. Stevens, and W. R. Cotton, 1996: Effects of aerosols and horizontal inhomogeneity on the broadband albedo of marine stratus: Numerical simulations. *J. Atmos. Sci.,* **53,** 3757–3769.

Fischer, J., and H. Grassl, 1991: Detection of cloud-top height from backscattered radiances within the oxygen A band. Part I: Theoretical study. *J. Appl. Meteor.,* **30,** 1245–1259.

Fouquart, Y., and B. Bonnel, 1980: Computations of solar heating of the Earth's atmosphere: A new parameterization. *Beitr. Phys. Atmos.,* **53,** 35–62.

——, J. C. Buriez, M. Herman, and R. S. Kandel, 1990: The influence of clouds on radiation: A climate-modeling perspective. *Rev. Geophys.,* **28,** 145–166.

Gultepe, I., G. A. Isaac, W. R. Leaitch, and C. M. Banic, 1996: Parameterizations of marine stratus microphysics based on in situ observations: Implications for GCMs. *J. Climate,* **9,** 345–357.

Han, Q., W. B. Rossow, and A. A. Lacis, 1994: Near-global survey of effective droplet radii in liquid water clouds using ISCCP data. *J. Climate,* **7,** 465–497.

Hansen, J. E., and L. D. Travis, 1974: Light scattering in planetary atmospheres. *Space Sci. Rev.,* **16,** 527–610.

Jones, A., D. L. Roberts, and A. Slingo, 1994: A climate model study of indirect radiative forcing by anthropogenic sulphate aerosols. *Nature,* **370,** 450–453.

King, M. D., L. F. Radke, and P. V. Hobbs, 1990: Determination of the spectral absorption of solar radiation by marine stratocumulus clouds from airborne measurements within clouds. *J. Atmos. Sci.,* **47,** 894–907.

——, ——, and ——, 1993: Optical properties of marine stratocumulus clouds modified by ships. *J. Geophys. Res.,* **98,** 2729–2739.

Langner, J., and H. Rodhe, 1991: A global three-dimensional model of the tropospheric sulfur cycle. *J. Atmos. Chem.,* **13,** 225–263.

Le Treut, H., and Z. X. Li, 1991: Sensitivity of an atmospheric general circulation model to prescribed SST changes: Feedback effects associated with the simulation of cloud optical properties. *Climate Dyn.,* **5,** 175–187.

Li, J., J. W. Geldart, and P. Chýlek, 1994: Solar radiative transfer in clouds with vertical internal inhomogeneity. *J. Atmos. Sci.,* **51,** 2542–2552.

McFarlane, N. A., G. J. Boer, J.-P. Blanchet, and M. Lazare, 1992: The Canadian Climate Centre second-generation general circulation model and its equilibrium climate. *J. Climate,* **5,** 1013–1044.

Martin, G. M., D. W. Johnson, and A. Spice, 1994: The measurement and parameterization of effective radius of droplets in warm stratocumulus clouds. *J. Atmos. Sci.,* **51,** 1823–1842.

——, ——, P. R. Jonas, D. P. Rogers, I. M. Brooks, and R. W. Barlow, 1997: Effects of airmass type on the interaction between warm stratocumulus and underlying cumulus clouds in the marine boundary layer. *Quart. J. Roy. Meteor. Soc.,* **123,** 849–882.

Nakajima, T., and M. D. King, 1990: Determination of the optical thickness and effective particle radius of clouds from reflected solar radiation measurements. Part I: Theory. *J. Atmos. Sci.,* **47,** 1878–1893.

——, ——, J. D. Spinhirne, and L. F. Radke, 1991: Determination of the optical thickness and effective particle radius of clouds from reflected solar radiation measurements. Part II: Marine stratocumulus observations. *J. Atmos. Sci.,* **48,** 728–750.

Nicholls, S., 1984: The dynamics of stratocumulus: Aircraft observations and comparisons with a mixed layer model. *Quart. J. Roy. Meteor. Soc.,* **110,** 783–820.

Parol, F., J. Descloitres, and Y. Fouquart, 2000: Cloud optical thickness and albedo retrievals from bidirectional reflectance measurements of POLDER instruments during ACE-2. *Tellus,* in press.

Pawlowska, H., and J. L. Brenguier, 1996: A study of the microphysical structure of stratocumulus clouds. *Proc. 12th Int. Conf. on Clouds and Precipitation,* Zurich, Switzerland, International Commission on Clouds and Precipitation (ICCP) and International Association of Meteorology and Atmospheric Science (IAMAS), 23–26.

——, and ——, 2000: Microphysical properties of stratocumulus clouds during ACE2. *Tellus,* in press.

Pelon, J., P. H. Flamant, C. Flamant, R. Valentin, G. Megie, and M. Meissonnier, 1992: The airborne lidar LEANDRE 1. *Proc. Specialty Meeting on Airborne Geoscience,* Toulouse, France, Météo-France, INSU, and CNES, 143–146.

——, C. Flamant, V. Trouillet, and P. H. Flamant, 2000: Optical and microphysical parameters of dense stratocumulus clouds during mission 206 of EUCREX'94 as retrieved from LEANDRE 1 measurements. *Atmos. Res.,* in press.

Pincus, R., and M. B. Baker, 1994: Effect of precipitation on the albedo susceptibility of clouds in the marine boundary layer. *Nature,* **372,** 250–252.

Plass, G. N., G. W. Kattawar, and F. E. Catchings, 1973: Matrix operator theory of radiative transfer. 1: Rayleigh scattering. *Appl. Opt.,* **12,** 314–329.

Platnick, S., and S. Twomey, 1994: Determining the susceptibility of cloud albedo to changes in droplet concentration with the advanced very high resolution radiometer. *J. Appl. Meteor.,* **33,** 334–347.

——, and F. P. J. Valero, 1995: A validation of satellite cloud retrieval during ASTEX. *J. Atmos. Sci.,* **52,** 2985–3001.

Pontikis, C. A., 1996: Parameterization of the droplet effective radius of warm layer clouds. *Geophys. Res. Lett.,* **23,** 2629–2632.

——, and E. Hicks, 1992: Contribution to the cloud droplet effective radius parameterization. *Geophys. Res. Lett.,* **19,** 2227–2230.

Raes, F., and T. Bates, 1995: ACE-2 science and implementation plan. Office for Official Publications of the European Communities Rep. CL-NA-16229-EN-C.

Raga, G. B., and P. R. Jonas, 1993a: Microphysical and radiative properties of small cumulus clouds over the sea. *Quart. J. Roy. Meteor. Soc.,* **119,** 1399–1417.

——, and ——, 1993b: On the link between cloud-top radiative properties and sub-cloud aerosol concentrations. *Quart. J. Roy. Meteor. Soc.,* **119,** 1419–1425.

Randall, D. A., J. A. Coakley Jr., C. W. Fairall, R. A. Kropfli, and D. H. Lenschow, 1984: Outlook for research on subtropical marine stratiform clouds. *Bull. Amer. Meteor. Soc.,* **65,** 1290–1301.

Rawlins, F., and J. S. Foot, 1990: Remotely sensed measurements of stratocumulus properties during FIRE using the C130 aircraft Multi-Channel Radiometer. *J. Atmos. Sci.,* **47,** 2488–2503.

Rosenfeld, D., and I. M. Lensky, 1998: Satellite-based insights into precipitation formation processes in continental and maritime convective clouds. *Bull. Amer. Meteor. Soc.,* **79,** 2457–2476.

Schüller, L., J. Fischer, W. Armbruster, and B. Bartsch, 1997: Calibration of high resolution remote sensing instruments in the visible and near infrared. *Adv. Space. Res.,* **19,** 1325–1334.

——, W. Armbruster, and J. Fischer, 2000: Retrieval of cloud optical and microphysical properties from multi-spectral radiances. *Atmos. Res.,* in press.

Slingo, A., 1989: A GCM parameterization for the shortwave radiative properties of water clouds. *J. Atmos. Sci,* **46,** 1419–1427.

——, 1990: Sensitivity of the Earth's radiation budget to changes in low clouds. *Nature,* **343,** 49–51.

——, and H. M. Schrecker, 1982: On the shortwave radiative properties of stratiform water clouds. *Quart. J. Roy. Meteor. Soc.,* **108,** 407–426.

——, S. Nicholls, and J. Schmetz, 1982: Aircraft observations of marine stratocumulus during JASIN. *Quart. J. Roy. Meteor. Soc.,* **108,** 833–856.

Stephens, G. L., 1978: Radiation profiles in extended water clouds. II: Parameterization schemes. *J. Atmos. Sci.,* **35,** 2123–2132.

——, and C. M. R. Platt, 1987: Aircraft observations of the radiative and microphysical properties of stratocumulus and cumulus cloud fields. *J. Climate Appl. Meteor.,* **26,** 1243–1269.

——, and S. Tsay, 1990: On the cloud absorption anomaly. *Quart. J. Roy. Meteor. Soc.,* **116,** 671–704.

Taylor, J. P., and A. McHaffie, 1994: Measurements of cloud susceptibility. *J. Atmos. Sci.,* **51,** 1298–1306.

Twomey, S., 1977: The influence of pollution on the shortwave albedo of clouds. *J. Atmos. Sci.,* **34,** 1149–1152.

——, 1991: Aerosols, clouds and radiation. *Atmos. Environ.,* **254,** 2435–2442.

——, and T. Cocks, 1989: Remote sensing of cloud parameters from spectral reflectance measurements in the near-infrared. *Beitr. Phys. Atmos.,* **62,** 172–179.

——, H. Jacobowitz, and H. B. Howell, 1966: Matrix methods for multiple scattering problems. *J. Atmos. Sci.,* **23,** 101–108.

van de Hulst, H. C., 1957: *Light Scattering by Small Particles.* John Wiley and Sons, 470 pp.